Effect of carbon coating on surface structure in annealing process of high-dose implanted/annealed SiC

Ishiji, Kotaro
SAGA Light Source

Arita, Makoto
Department of Materials Science and Engineering, Kyushu University

Adachi, Mariko
Nanophoton Corporation

Sugie, Ryuichi
Toray Research Center, Inc.

他

https://hdl.handle.net/2324/7218269

出版情報：Journal of Applied Physics. 135 (18), pp.185703-1-185703-10, 2024-05-08. AIP Publishing
バージョン：

Journal of Applied Physics

RESEARCH ARTICLE | MAY 08 2024

Effect of carbon coating on surface structure in annealing process of high-dose implanted/annealed SiC

Special Collection: Defects in Semiconductors 2024

Kotaro Ishiji ✉ ; Makoto Arita ; Mariko Adachi ; Ryuichi Sugie ; Yukihiro Morita ; Tsutomu Araki

Check for updates

J. Appl. Phys. 135, 185703 (2024)
https://doi.org/10.1063/5.0205320

View Online

Export Citation

AIP Publishing

Journal of
Applied Physics ARTICLE pubs.aip.org/aip/jap

Effect of carbon coating on surface structure in annealing process of high-dose implanted/annealed SiC

Cite as: J. Appl. Phys. **135**, 185703 (2024); doi: 10.1063/5.0205320
Submitted: 25 February 2024 · Accepted: 22 April 2024 ·
Published Online: 8 May 2024

Kotaro Ishiji,[1,a)] Makoto Arita,[2] Mariko Adachi,[3] Ryuichi Sugie,[4] Yukihiro Morita,[5]
and Tsutomu Araki[6]

AFFILIATIONS

[1]SAGA Light Source, 8-7 Yayoigaoka, Tosu, Saga 841-0005, Japan
[2]Department of Materials Science and Engineering, Kyushu University, 744 Motooka, Nishi-ku, Fukuoka 819-0395, Japan
[3]Nanophoton Corporation, 3-1-7 Funabanishi, Mino, Osaka 562-0036, Japan
[4]Toray Research Center, Inc., 3-2-11 Sonoyama, Otsu, Shiga 520-8567, Japan
[5]Ion Technology Center Co., Ltd., 2-8-1 Tsudayamate, Hirakata, Osaka 573-0128, Japan
[6]Ritsumeikan University, Department of Electrical and Electronic Engineering, 1-1-1 Noji-Higashi, Kusatsu, Shiga 525-8577, Japan

Note: This paper is part of the special topic, Defects in Semiconductors 2024.

[a)]**Author to whom correspondence should be addressed:** ishiji@saga-ls.jp

ABSTRACT

The effect of carbon coating on a surface structure of a high-dose implanted/annealed silicon carbide (SiC) during annealing was examined using scanning probe microscopy (SPM), deep-ultraviolet (DUV) Raman spectroscopy, and transmission electron microscopy (TEM). In SPM, the surfaces of 500- and 30 °C-implanted/annealed SiC samples without coating exhibited a periodic-step structure and granular structure, respectively. The difference between these surfaces is attributed to the absence or presence of residual implantation damage. In contrast, surface flatness was maintained in the 500 °C-implanted/annealed SiC sample with carbon coating. However, the surface of the coated 30 °C-implanted/annealed SiC sample exhibited a geometric structure with a lattice pattern parallel to the $\langle 11\bar{2}0\rangle$ axes. The DUV Raman spectra and TEM images indicated that the implanted layer of this sample metamorphosed into a mixture of 3C-SiC twin domains and amorphous-SiC regions. During the cooling process after annealing, the 3C-SiC region was more raised than the amorphous-SiC region owing to the difference in the thermal expansion coefficients, thus resulting in the generation of a geometric surface structure. In the metamorphosed implanted layer, the carbon coating does not completely prevent surface roughening.

I. INTRODUCTION

Silicon carbide (SiC) power devices, such as SiC diodes and transistors, are currently being developed by researchers. Impurity doping via ion implantation is essential for device processing and is crucial in the realization of high-performance SiC devices. As implantation damages the crystal structure, annealing at temperatures exceeding 1500 °C is typically performed for crystal recovery. SiC crystals are electrically activated through implantation and annealing. However, the surface may result in rough depending on implantation and annealing conditions. Capano *et al.*[1] showed that atoms emitted by annealing returned to the surface of SiC and developed into macro-steps by adsorbing atoms in the off-angle direction. The surface macro steps grow with the annealing temperature and annealing time.[2,3] Surface structures roughened by annealing-induced step bunching are undesirable as they deteriorate the performance of SiC devices.[2] To avoid step bunching, a surface coating technique prior to annealing was proposed.[4] Annealing involving a carbon coating can maintain the surface flatness without increasing roughness in implanted/annealed SiC with a dose of $1\times10^{16}\,\mathrm{cm}^{-2}$ ($\sim5\times10^{20}\,\mathrm{cm}^{-3}$).[5] Rapid thermal annealing, a short annealing technique that persists less than several minutes, is similarly effective in alleviating surface roughness.[6,7] On a SiC surface, the crystallinity of Si nanocrystals in rapid thermal annealing is higher than that in furnace annealing.[8] Currently, carbon coatings and rapid thermal annealing are widely employed for implanted/annealed SiC to prevent an increase in surface roughness.

High-dose implantation ($\sim 10^{20}$ cm^{-3}) is typically performed using advanced SiC fabrication techniques to create a dopant-concentration gradient. However, this causes significant damage to the crystals. The implanted layer of SiC is amorphized during high-dose implantation at a low temperature despite subsequent annealing.[9–11] With regard to the heavy implantation of SiC, Weber and Gao[12] suggested the introduction of clustered defects and solid-state amorphization by collapsing the crystal lattice. Defect clusters and stacking faults have been confirmed as residual implantation suffers damage under heavy implantation.[13,14] Implantation damage adversely affects the electrical properties of SiC. In a high-dose implanted/annealed SiC achieved at 30 °C, we discovered residual implantation damage and observed high resistivity.[15,16] Furthermore, heavy implantation damage increased the surface roughness. Canino *et al.*[17,18] confirmed that the surface roughness of high-dose implanted/annealed SiC samples increased, despite the application of a carbon layer during annealing. Depending on the implantation and annealing conditions, maintaining the surface flatness can be challenging even when the surface is coated with a carbon layer during annealing.

Studies regarding the surface structure of SiC in carbon coatings are useful for optimizing the processing of SiC devices. This is because different SiC fabrication methods require different implantation and annealing conditions as well as different requirements for surface roughness. In a simulation using a physical model for SiC fabrication, a roughened surface structure limited channel mobility in the subthreshold and linear regions of device operation under high gate biases.[19] Canino *et al.*[17,18] reported the surface roughness of implanted/annealed SiC with carbon coating as a function of the implantation dose or annealing temperature, which provided valuable results for SiC fabrication. The SiC crystal state of the implanted layer was reported to depend on the implantation temperature.[20–23] The surface structure is assumed to be affected by the crystal state of an implanted layer. Hence, the effect of carbon coating on the surface structure of a high-dose implanted/annealed SiC must be investigated.

In this study, we prepared high-dose implanted/annealed SiC samples at different implantation temperatures. To examine the effect of carbon coating on the surface structure, implanted samples with and without carbon coating were prepared and subjected to high-temperature annealing. The surface structure, lattice periodic order, and fine structure visualization of the implanted layers in the prepared samples were evaluated using scanning probe microscopy (SPM), deep-ultraviolet (DUV) Raman spectroscopy, and transmission electron microscopy (TEM), respectively. SPM was widely used to observe the surface morphology of the SiC crystals. Negoro *et al.*[5] clarified the suppression effect of surface roughness caused by carbon coating using SPM. The surface structure might be caused by the crystal structure of the implanted layer, and a discussion regarding its relationship with the crystal structure of the implanted layer is required. Raman spectroscopy is widely used to evaluate SiC crystal lattice structures. Harima[24] characterized the attribution of the lattice structure to SiC Raman peaks. TEM is an effective tool for observing fine SiC structures. For example, TEM images show the residual damage, such as voids and stacking faults, in the implanted layer of SiC.[14] These approaches are effective for the structural evaluation of the implanted SiC layer and are suitable for satisfying the purpose of this study. By investigating the crystal structure in the implanted layer, we discuss the behavior of the surface structures of high-dose implanted/annealed SiC samples with and without carbon coating.

II. EXPERIMENTS

Four commercial epitaxial 4H-SiC(0001) chip samples with an off-cut axis of 4° in the $[11\bar{2}0]$ direction were used. The thickness of the epilayer was 10 μm, and the sample size was $10 \times 10 \times 0.35$ mm^3. The designed box-type phosphorus ions (P^+) were implanted with a 4×10^{20} cm^{-3} dose using a 200 keV-class implanter (NH-20SR: Nisshin Ion Equipment Co. Ltd.).[25] The sample was mounted on a platen stage of a heater in the instrument. Subsequently, P ions were implanted normal to the surface of the sample. For box-type implantation, acceleration energies of 15, 35, 60, 100, and 180 keV were applied. The implantation temperatures were 30 and 500 °C each, for two samples. The implantation temperature was controlled to 500 ± 5 °C to maintain accuracy. During the implantation, the inside of the instrument was maintained under high vacuum ($\sim 10^{-6}$ Pa). Figure 1 shows the implantation dose and damage profiles vs the implantation depth based on the stopping and range of ions in the matter (SRIM) calculation code. For these calculations, the implantation temperature was assumed to be the room temperature (~30 °C). The implanted P ions were uniformly distributed at a dose of 4×10^{20} cm^{-3} and decreased rapidly at more than 200 nm depth. The implantation damage was estimated to be approximately 0.33 displacements per atom (DPA) at the maximum.

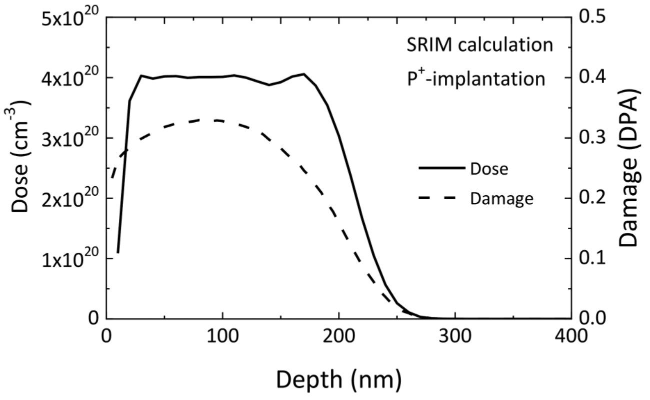

FIG. 1. Dose and damage vs P^+-implantation based on SRIM calculation. Dose and damage are indicated on left and right axes, respectively. Implantation temperature is assumed to be room temperature (~30 °C) in the calculations.

TABLE I. Details pertaining to sample name, implantation temperature, annealing temperature, and absence or presence of carbon coating during annealing.

Sample name	NC1	NC2	WC1	WC2
Implantation temperature (°C)	500	30	500	30
Annealing temperature (°C)	1600 (no coating)		1600 (with coating)	

After implantation, one 30 °C-implanted SiC sample and one 500 °C-implanted SiC sample were coated with a 100-nm-thick diamond carbon (DLC) layer using a plasma-based deposition system (PBII series: Kurita Manufacturing Co. Ltd.) under an acetylene reaction.[26] The deposition rate was 7 nm/min and the layer was expected to be uniform. The coated DLC was a hydrogenated type similar to the graphite structure and guaranteed to withstand temperature exceeding 2000 °C during annealing. Before annealing, the complete coverage of the surface with a carbon layer was confirmed under a microscope. Subsequently, all the implanted SiC samples were annealed at 1600 °C for 5 min in an argon gas atmosphere using a thermal annealing furnace, which is a typical rapid thermal annealing process. The annealing was achieved at a heating rate of 500 °C/min followed by natural cooling. During annealing, the temperature change was controlled within 0.5%. The effect of the annealing error on the results was negligible owing to the accurate temperature control. The heavily P$^+$-implanted SiC was sufficiently activated via annealing at 1600 °C.[16] Table I presents the correspondence among the sample number, implantation temperature, annealing temperature, and absence or presence of carbon coating. Samples NC1 and NC2 were annealed without the coating, whereas samples WC1 and WC2 were annealed with carbon coating. After annealing in a thermal oxidation furnace, the carbon coating of WC1 and WC2 was completely removed in an oxygen atmosphere at 800 °C for 120 min. During the coating-removal process, carbon combined with oxygen and evaporated as carbon dioxide. Subsequently, WC1 and WC2 were cleaned using a 5% hydrofluoric acid solution in a fume hood. Finally, the cleaned surface without carbon coating was achieved via microscopy. An un-implanted SiC sample (R0) was used as a reference. Implantation, carbon coating, annealing, and coating removal processes were performed at the Ion Technology Center Co. Ltd. These implantation and annealing procedures were performed as standard procedures for SiC fabrication.

The surface morphologies of the prepared samples were measured via SPM (Model 5400: Agilent Technologies Inc.) at Kyushu University. The sample was mounted on a vibration isolation table, and the resonance frequency of the cantilever was tuned using laser. The resonance frequency and amplitude of the cantilever were 300 kHz and 1.5 V, respectively. Then, the cantilever approached the sample surface, and the surface was probed in the tapping mode. SPM observations were conducted in a clean room. The surfaces of the prepared samples were probed before and after annealing. The probed area measured $5 \times 5\,\mu\mathrm{m}^2$ and the pixel size was $20 \times 20\,\mathrm{nm}^2$. The output pixel data were edited into a two-dimensional image, and the root mean square (RMS) roughness value of the observed area was analyzed.

DUV Raman spectroscopy was performed using a Raman spectrometer (RAMANtouch vioLa: Nanophoton Corp.) at the Nanophoton Corporation to evaluate the lattice order of the implanted layers of the prepared samples. The sample was placed on a stage, and then an excitation laser was focused on the sample surface using a microscope. The laser head wavelength and power were 266 nm and 50 mW, respectively. The laser was focused on the sample surface using a 40× objective lens (numerical aperture: 0.5), and the Raman scattering light was corrected in a backscattering geometry. The probed light from the sample was captured using a cooled charge-coupled device detector. The pixel resolution of the wavenumber was 0.9 cm^{-1} with 3600 gr/mm in grating. The measurements were performed 10 times with an exposure time of 3 min. The probing depth of the DUV laser was estimated to be approximately 200 nm,[24] which reflected the signal of the implanted layer in the Raman data.

Cross-sectional TEM was performed on the NC2 and WC2 samples. The sample must be thin to allow the electron beam to transmit through the sample. First, the samples were cut across the center along the $[11\bar{2}0]$ axis. Subsequently, a 100-nm-thick cross section of the sample was designed using a focused ion beam. The designed sample was mounted on a TEM holder and transferred to the observation position. Subsequently, the fine structure of the implanted layer in the cross-sectional $(\bar{1}100)$ plane was observed using a TEM system (JEM-2100 Plus: JEOL Ltd.) at Ritsumeikan University. The accelerating voltage was 200 kV and the current was 0.1 mA. The samples were placed at the focal beam position in a vacuum chamber. The inside of the chamber was maintained under high vacuum ($\sim 10^{-6}$ Pa). A charge-coupled device detector was used to obtain the bright-field and diffraction images. The size of the detector was 2048×2048 pixels.

III. RESULTS

A. SPM image

Figure 2 shows the SPM image of the surface structure for (a) the un-implanted SiC sample (R0), (b) sample as-implanted at 30 °C, (c) sample as-implanted at 500 °C, (d) NC1 after annealing, (e) NC2 after annealing, (f) WC1 after annealing, and (g) WC2 after annealing. The surface structure of R0 [see Fig. 2(a)] was smooth and the RMS roughness was less than 1 nm, which is characteristic of the surface morphology of an epitaxial-grown crystal.[27] In Figs. 2(b) and 2(c), the surface morphologies and RMS roughness values of the as-implanted SiC samples were similar to those of R0. The surface structure remained almost unchanged despite the heavy implantation, which is consistent with the results reported in Ref. 4.

After annealing, the surface of the NC1 surface exhibited a stepwise structure, as shown in Fig. 2(d). The step spacing and RMS roughness were 1 μm and more than 4 nm, respectively. Annealing without coating evaporated the surface atoms, and some of the emitted atoms returned to the surface. The returned atoms migrated across the surface and were eventually trapped in the step by the off-angle.[1,2] This event occurred repeatedly, thereby resulting in a step-bunching structure. Although the implantation and annealing conditions were slightly different, Negoro *et al.*[5] observed a step-bunching surface on implanted/annealed SiC without

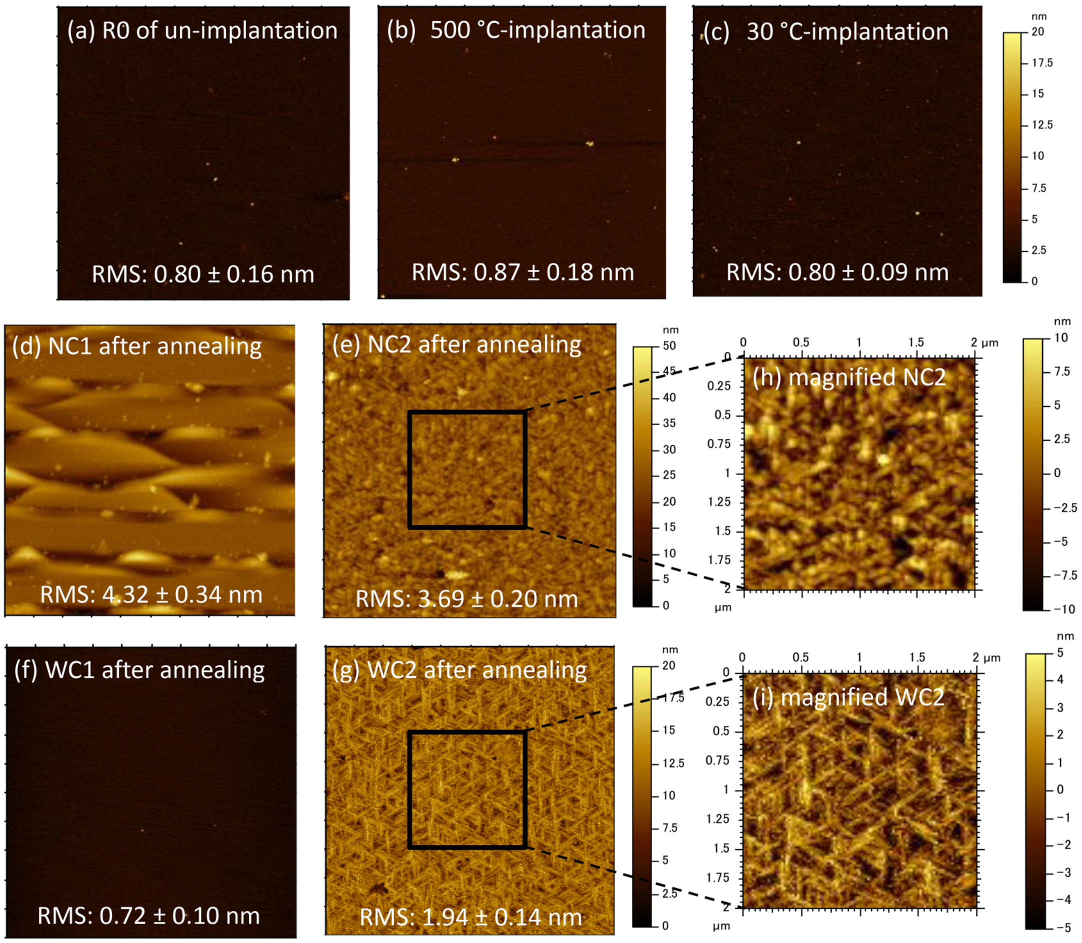

FIG. 2. SPM images of prepared SiC samples measuring 5 × 5 μm^2; (a) R0 in an un-implanted state, (b) SiC as-implanted at 500 °C, (c) SiC as-implanted at 30 °C, (d) NC1 after annealing, (e) NC2 after annealing, (f) WC1 after annealing, and (g) WC2 after annealing. (h) and (i) show magnified SPM images in 2 × 2 μm^2 of (e) and (g), respectively. The Z-scale bar is shown on the right side in each image; (a) and (b) are the same as (c); (d) is the same as (e); and (f) is the same as (g). The average RMS roughness probed in three areas is shown in (a)–(g).

coating. The surface structure reported was similar to that shown in Fig. 2(d). The surface of NC2 after annealing, as shown in Fig. 2(e), was similarly roughened; however, it exhibited a random granular structure instead of a step-bunching structure. This indicates that the step-bunching event described above did not occur on the surface of NC2. Canino *et al.*[17] observed a granular surface on implanted/annealed SiC. Their granular surface were similar to that shown in Fig. 2(e). The difference between the surface structures of NC1 and NC2 can be attributed to the crystal state of the implanted layer. The high-temperature implantation contributed to the competitive prerecovery of the implantation damage.[20,21] In NC1, the 4H-lattice structure was barely maintained owing to the prerecovery at 500 °C during implantation. Subsequent annealing almost completely recovered the 4H-structure, thus resulting in a step structure on the surface. In contrast, in NC2, the 4H-lattice structure was completely lost during implantation owing to the low implantation temperature of 30 °C. Severe damage persisted despite subsequent high-temperature annealing. The residual damage may have resulted in the formation of the granular surface structure shown in Fig. 2(e). In a previous study, we visually ascertained the maintained 4H structure of the same implanted SiC as NC1 and the lost 4H structure of the implanted SiC as NC2.[23] In the heavily implanted SiC sample at a low implantation temperature, the residual implantation damage was severe and transformed the crystal state after annealing.[28] In NC2, the crystal state metamorphosed and step bunching did not occur, thus resulting in the development of the granular surface structure.

The WC1 surface shown in Fig. 2(f) was as flat as the R0 surface. The surface of WC1 was coated with a carbon layer, and no atoms were emitted during annealing. The flatness of the surface was maintained because of carbon coating. The implanted layer of WC1 maintained a 4H-structure similar to that of NC1, and step-bunching behavior was prevented by carbon coating. The flat surface shown in Fig. 2(f) was similar to the surface of the implanted/annealed SiC with carbon coating in Ref. 5. In contrast, the surface of WC2 after annealing [Fig. 2(g)] was roughened despite the presence of the carbon coating. The RMS roughness value was half that of NC2. A roughened surface on the implanted/annealed SiC was reported despite the application of surface coating during annealing.[17,18,28] The implantation damage that remained in the implanted layer of WC2 was similar to that of NC2 because of the low implantation temperature of 30 °C. However, in WC2, the surface roughness was not completely prevented despite the presence of carbon coating during annealing. Figures 2(h) and 2(i) show the magnified images of Figs. 2(e) and 2(g), respectively. The surface structure in Fig. 2(h) exhibited random granularity, whereas a unique lattice pattern was observed in Fig. 2(i). The straightline segments of the lattice pattern, which measured ~0.3 μm long and ~0.05 μm wide, were parallel to the $\langle 11\bar{2}0\rangle$ [= $(11\bar{2}0)$, $(1\bar{2}10)$, and $(\bar{2}110)$] axes, and relatively raised compared with the average surface. This pattern is unique because it reflects the lattice structure of SiC. Similar to NC2, WC2 should contain residual damage in the implanted layer. However, the reabsorption of evaporated atoms, similar to the case of NC2, did not occur in WC2 because its surface was coated with a carbon layer. The difference between NC2 and WC2 was the absence or presence of carbon coating during annealing. Hence, the absence or presence of carbon coating was assumed to have contributed to the unique geometric structure of WC2.

B. Raman spectrum

Figure 3 shows the DUV Raman spectra of: (a) as-implanted NC1, NC2, WC1, and WC2 and (b) after they were annealed. The Raman spectrum of R0 is shown in gray for reference. In the R0 spectrum, sharp peaks were observed at 610, 776, 798, 838, and 965 cm^{-1}, which were attributed to the oscillation folded longitudinal acoustic [FLA(A_1)], folded transverse optical [FTO(E_2)], transverse optical [TO(E_1)], folded longitudinal optical [FLO(A_1)], and longitudinal optical [LO(A_1)] modes, respectively.[29,30] The R0 spectrum is regarded as a typical spectrum of commercial 4H-SiC. In the Raman spectrum of the SiC as-implanted at 30 °C, a flat profile without a peak was observed. The implanted layer of the SiC as-implanted at 30 °C was considered to have lost its periodic lattice order. This is supported by the loss of lattice bonding in the as-implanted SiC under the same condition in the x-ray topograph.[23] The spectrum of the SiC as-implanted at 500 °C did not show a peak but indicated a small broad intensity at 740−960 cm^{-1}. In a previous study, a similar broad intensity was observed at 740−960 cm^{-1} in the Raman spectrum of the SiC as-implanted at 500 °C.[15] Furthermore, in the x-ray topograph, the evidence of residual lattice bonding was obtained in the as-implanted SiC under the same condition.[23] Thus, the small broad intensity was assumed to be a trace of the 4H-structure maintained by the prerecovery effect of the high-temperature implantation. The surface atoms neither evaporated nor reabsorbed owing to carbon coating in annealing, although the lattice order in the implanted layer was almost lost during the implantation. Therefore, no changes were observed in the surface morphology, as shown in Figs. 2(b) and 2(c).

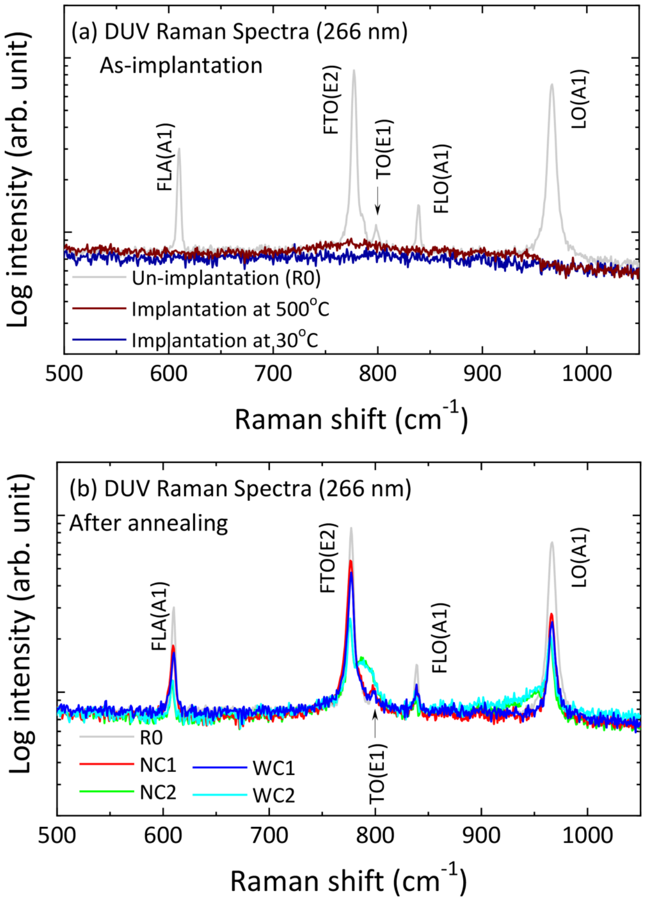

FIG. 3. DUV Raman spectra; (a) SiC samples as-implanted at 500 and 30 °C and (b) NC1, NC2, WC1, and WC2 after annealing. DUV Raman spectrum of R0 is shown as a reference in (a) and (b). Raman modes of 4H-SiC are shown in (a) and (b).

As shown in Fig. 3(b), Raman peaks appeared in all the samples after annealing. The spectra of NC1 and WC1 were similar to the R0 spectrum. This means that the 4H-structures of the implanted layers of NC1 and WC1 were almost completely recovered. Despite the different surface morphologies of NC1 and WC1, the lattice structures of the implanted layers were identical. This indicates that the Raman signal was insensitive to the surface structure. Meanwhile, NC2 and WC2 showed peaks at 610, 776, 798, 838, and 965 cm^{-1} as a 4H-structure. However, the peak intensities of the 4H-structure were weak, whereas a broad peak at 790 cm^{-1} and a broad intensity at 880−960 cm^{-1} newly appeared. The peak at 790 cm^{-1} was in close proximity to the TO peak of a typical 3C-SiC.[29] Heavy implantation into a SiC crystal has been reported to generate a polytype 3C-structure.[31–34] Therefore, the unusual increased intensity of NC2 and WC2 at 790 cm^{-1} was expected to be caused by the formation of 3C-SiC. Meanwhile, a significant amount of implantation damage has been reported to destroy the periodic stacking sequence of the lattice structure.[35] In a previous study, we reported increased Raman intensity at 880–960 cm^{-1} in an implanted/annealed SiC sample with the same specifications as NC2.[13] Nakashima *et al.*[36] suggested that broad Raman intensity appeared at 880–960 cm^{-1} because of the presence of an amorphous-SiC state. The formation of amorphous-SiC relaxed the Raman selection rule, thus resulting in broad intensity. Excess implantation damage did not allow the recovery of the 4H-structure even after high-temperature annealing, which might have caused the structural metamorphization of the implanted layer. The Raman spectra of NC2 and WC2 almost overlapped. This means that the implanted layers of NC2 and WC2 presented similar lattice structures. The Raman spectra of NC2 and WC2 showed that the absence or presence of carbon coating did not interfere with the structure of the implanted layer.

C. TEM image

Figures 4(a) and 4(b) show the cross-sectional TEM images of the implanted layer in NC2 and WC2 after annealing, respectively. The interface between the epilayer and the implanted layer was observed at 200 nm from the surface. The uniform contrast of the epilayers indicated favorable crystallinity. However, the implanted layer exhibited a nonuniform contrast. This indicates the inferior crystallinity of the implanted layer, which was attributed to residual

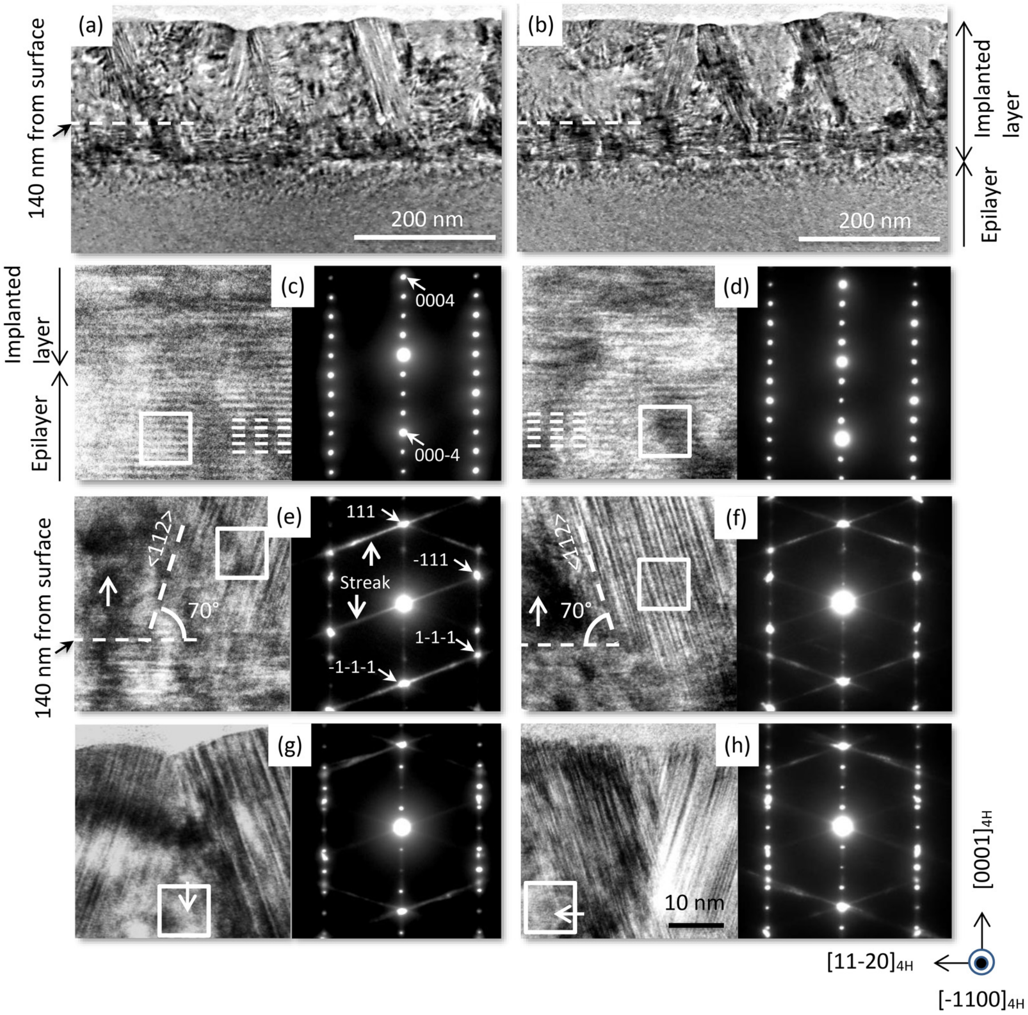

FIG. 4. Cross-sectional TEM images of implanted/annealed SiC; (a) entire implanted layer of NC2, (b) entire implanted layer of WC2, (c) epilayer/implanted layer interface of NC2, (d) epilayer/implanted layer interface of WC2, (e) depth of 140 nm from the surface of NC2, (f) depth of 140 nm from the surface of WC2, (g) near the surface of NC2, and (h) near the surface of WC2. Scale factors in (c)–(h) are the same. In (c)–(h), bright-field and diffraction images are shown on the left and right sides, respectively. The diffraction pattern reflects an enclosed square area of the bright-field image in each image. Subscript "4H" indicates a 4H-structure.

damage caused by implantation. Furthermore, in the implanted layer, the upper- and lower-half regions indicated different crystallinities at a depth of 140 nm (as the boundary), as indicated by the dotted line. In the upper-half region, two different crystal states were observed: one in the domain region with an inclination of 70° with respect to the *c*-plane, and the other in the blurred featureless region between the domains. Blurred fringes parallel to the (0001) plane were observed in the lower-half region. The findings above were similarly observed in both NC2 and WC2.

Figures 4(c) and 4(d) show magnified TEM images at the interface of the epilayer/implanted layer in NC2 and WC2, respectively. Regularly aligned fringes were observed in the lower half of the bright-field images (the epilayer region). The stripes, as indicated by the dotted lines, were parallel to the (0001) plane at regular intervals. The diffraction images enclosed by the square area are shown on the right-hand sides of Figs. 4(c) and 4(d). In both diffraction images, regular spots with four periods along the $\langle 0001\rangle$ axis were observed. The regular spot pattern indicates the typical pattern of a 4H-structure.[33] In contrast, a layer with blurred fringes was observed in the upper half of the bright-field images in Figs. 4(c) and 4(d). This region was located at the bottom of the implanted layer. Blurred fringes including a stacking sequence parallel to the *c*-plane have been reported at the bottom of the implanted layer in high-dose implanted/annealed SiC.[14,37–40] Thus, the blurred fringes shown in Figs. 4(a) and 4(b) were identified as stacking faults lying on the (0001) plane. Zhao *et al.*[41] suggested that the bottom region of the implanted layer was subjected to stress caused by defects, whereas the 4H-structure was maintained. Thus, the bottom region of the implanted layer barely maintained the 4H-structure, although it contained stacking faults.

Figures 4(e) and 4(f) show magnified TEM images at a depth of 140 nm from the surfaces of NC2 and WC2, respectively. Blurred fringes on the (0001) planes were observed in the lower half of the bright-field image. This region presented the same crystal state as the upper-half region, as shown in Figs. 4(c) and 4(d). Thus, the lower-half region shown in Figs. 4(e) and 4(f) included numerous implantation-induced stacking faults. In contrast, in the upper half of the bright-field images, the domains of the stacking sequence changing at ±70° with respect to the *c*-plane were observed. In the diffraction patterns shown on the left sides of Figs. 4(e) and 4(f), a periodic pattern with streaks across the zone axes was observed. The spot pattern was the same as that with respect to $\langle 01\bar{1}\rangle$ of a cubic structure,[34] and each spot was assigned a diffraction index reflecting the 3C-structure. Gorelik *et al.*[32] observed a 3C-twin structure on a blurred fringe layer in a high-dose implanted/annealed SiC. Furthermore, streaks across the zone axes have been reported to indicate the features of stacking faults.[31] Diani *et al.*[34] observed 3C-SiC twin domains with an inclination of 70° with respect to the (0001) plane in the implanted layer. Thus, the inclined angle of 70° corresponds to the $\langle 112\rangle$ axes of the 3C-structure. The 3C-SiC twin domains, as stable structures, were considered to have formed in the implanted layers of NC2 and WC2. Furthermore, fringes parallel to $\langle 112\rangle$ were observed inside the 3C-SiC domains. By performing x-ray topography, Vetter and Dudley.[42] observed stacking faults in a 3C-SiC crystal lying on $\{\bar{1}11\}$ habit planes. In a previous study, we obtained an x-ray topograph of stacking faults in the $\langle 110\rangle$ slip directions in 3C-SiC domains with $\{111\}$ twins on the on-axis of a 4H-SiC sample.[43] Thus, the fringes in the 3C-domain were identified as stacking faults parallel to $\langle 112\rangle$. In contrast, blurred featureless regions marked by arrows were observed adjacent to the 3C-SiC domain in Figs. 4(e) and 4(f). In this region, the contrast was blurred and uneven, thus indicating interior crystallinity.

Figures 4(g) and 4(h) show TEM images of the near-surface regions in NC2 and WC2, respectively. The 3C-SiC twin domain boundary was observed to have reached the surface. Additionally, blurred featureless regions (marked by arrows) were observed. These regions were similar to the featureless regions shown in Figs. 4(e) and 4(f). In the diffraction images of the featureless regions, the spots were irregularly spaced, similar to polycrystals with a mixture of 4H- and 3C-structures. Leclerc *et al.*[44] presented a TEM image that showed amorphization in an implanted SiC with

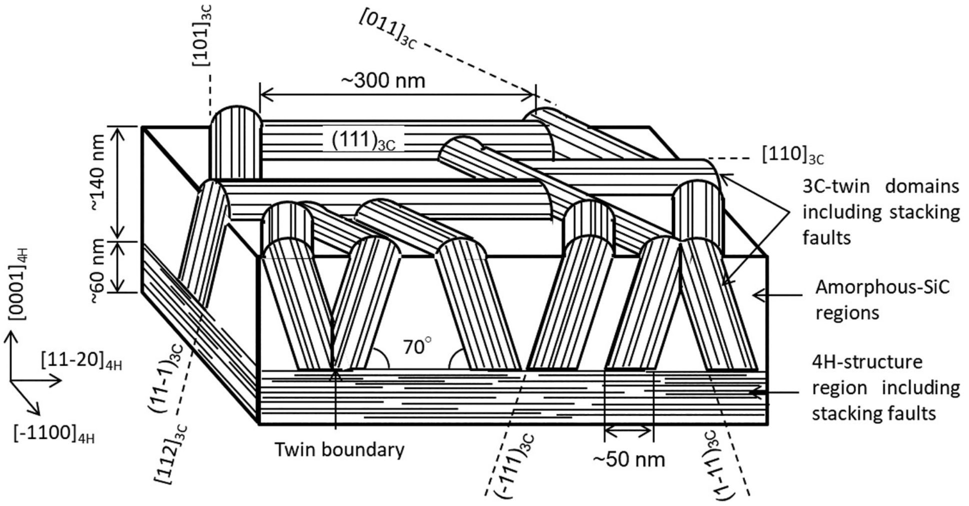

FIG. 5. Illustration of an implanted layer in WC2 after the removal of carbon coating. A 4H-structure with stacking faults occupies a region of depth 140–200 nm, whereas 3C-SiC twin domains with stacking faults and amorphous-SiC occupy a region of depth 140 nm from the surface. 3C-SiC domains are introduced parallel to the $\{\bar{1}11\}$ planes along $\langle 110\rangle$. Subscripts "4H" and "3C" indicate a 4H-structure and 3C-structure, respectively.

a high fluence of $2 \times 10^{16}\,\mathrm{cm}^{-2}$. In a TEM image, Zhao *et al.*[41] observed an amorphous layer induced by P-implantation at $1 \times 10^{15}\,\mathrm{cm}^{-2}$. Thus, the featureless region was identified as amorphous without a periodic lattice structure.

The implanted layer contained stacking faults, 3C-SiC twin domains, and amorphous-SiC regions. However, the fine structure of the implanted layer was the same for NC2 and WC2, and no differences were observed for both cases with and without carbon coating. The structure of the implanted layer was confirmed to be unaffected by the absence or presence of carbon coating, which is consistent with the Raman spectra shown in Fig. 3(b). Hence, we conclude that the unique geometric pattern shown in Fig. 2(i) was contributed by structural changes on the sample surface.

IV. DISCUSSION

We examined the relationship between the carbon coating and the surface structure of a high-dose implanted/annealed SiC. In the WC1 sample without residual damage, surface-roughness suppression by the carbon coating was confirmed. However, the surfaces of NC2 and WC2 with residual damage were roughened regardless of the absence or presence of carbon coating. Meanwhile, the surface morphologies of NC2 and WC2 were different despite having the same structure as the implanted layer. Therefore, the difference between the surface structures of NC2 and WC2 was derived from the absence or presence of carbon coating during annealing. In this section, we discuss the correlation between the absence or presence of carbon coating and the roughened surface structure. In particular, we focus on creating a geometric surface structure for WC2.

Figure 5 illustrates the assumed structure of the implanted layer in WC2, based on the obtained results. As shown by the TEM images in Fig. 4, in the blurred fringe region at a depth of 140−200 nm (at the bottom of the implanted layer), the 4H-structure was maintained, although extra stacking faults were introduced by implantation and annealing. The Raman peaks attributed to the 4H-structure of WC2 in Fig. 3(b) mainly reflected a blurred fringe region. At a region with more than 0.3 DPA in implantation damage, the 3C-SiC phase nucleated on the blurred fringe layer as a template after annealing.[32] Hence, 3C-twin domains were observed in the region at a depth of 140 nm from the surface, as shown in Fig. 4. In the Raman spectrum, the TO peak of 3C-SiC appeared at $796\,\mathrm{cm}^{-1}$.[29,45] Therefore, the broad Raman peak at $790\,\mathrm{cm}^{-1}$ in NC2 and WC2 shown in Fig. 3(b) is attributed to the mixture of the 3C-SiC TO peak and the peak edge of the 4H-SiC FTO(E_2) mode. The 3C-SiC domain presented a stacking sequence normal to the ⟨110⟩ directions, and stacking faults are typically introduced in the directions.[43,46] Marinova *et al.*[47] obtained cross-sectional TEM images that showed the formation of twin boundaries with $\{\bar{1}11\}$ stacking sequences in 3C-SiC. Yamashita *et al.*[48] presented a model of symmetric 3C-SiC twin domains with $\{\bar{1}11\}$ planes of the stacking sequence on 4H-SiC(0001). Therefore, 3C-SiC has stacking sequences parallel to the $\{\bar{1}11\}$ planes, including stacking faults in the ⟨110⟩ directions. As the (111) plane of the 3C-structure is coherent with the (0001) surface of 4H-SiC,[44,47] the $\langle 11\bar{2}0\rangle$ axes of the stripes in Fig. 2(i) correspond to ⟨110⟩ of the 3C-SiC twin domains. The width of the stripes in Fig. 2(i) was approximately 50 nm, which is consistent with the width of the 3C-SiC twin domains shown in Fig. 4. The 3C-SiC domains presented three ⟨110⟩ axes, with two symmetrical planes in each axis. A blurred featureless region was observed between the 3C-SiC domains shown in Fig. 4. This region was identified as amorphous-SiC composed of a mixture of 3C- and 4H-structures, based on the diffraction TEM patterns. The implanted layer of WC2 comprised a 4H-SiC layer with stacking faults, 3C-SiC twin domains, and amorphous-SiC regions.

The implanted layers of NC2 and WC2 were confirmed to have the same crystal state, although their surface morphologies differed. NC2 had a granular surface morphology owing to the reabsorption of the emitted atoms, whereas the surface atoms of WC2 did not evaporate because the surface was covered with a carbon layer. Therefore, the mixed structure comprising 3C-SiC and amorphous regions should be exposed on the surface of WC2 after coating removal. The 3C-SiC domains on the surface were relatively higher than those in the amorphous-SiC regions, as shown in Fig. 5. Furthermore, as shown in Fig. 4, the 3C-SiC domains appeared to be slightly higher on the sample surface. This can be explained by the difference in the thermal expansion coefficients of 3C-SiC and amorphous-SiC. The thermal expansion coefficients for 3C-SiC and amorphous-SiC were 3.5×10^{-6} and $5.3 \times 10^{-6}\,\mathrm{K}^{-1}$, respectively.[49,50] Thus, the WC2 sample cooled from 1600 °C to room temperature was reduced by 0.55% and 0.83% in volume for the 3C-SiC and amorphous-SiC regions, respectively. The implantation-induced swelling of SiC predominantly occurs in the *c*-axis direction.[22,23,51] After cooling to room temperature, the surface height was expected to be 2.5 nm lower and 3.8 nm lower for the 3C-SiC and amorphous-SiC regions, respectively. The difference in elevation between the 3C-SiC and the amorphous-SiC surfaces was 1.3 nm, and the value plus the intrinsic RMS roughness (∼0.8 nm) of the un-implanted state was consistent with the RMS roughness (1.94 nm) of WC2. The 3C-SiC domains were relatively elevated with respect to the amorphous regions because of the difference in their thermal expansion coefficients. After coating removal, the 3C-SiC domains in the ⟨110⟩ directions were exposed on the surface. Consequently, a unique geometric structure emerged on the WC2 surface. Stripes with bright contrast and spaces with dark contrast, as shown in Fig. 2(i), were observed and identified as metamorphosed 3C-SiC domains and amorphous-SiC regions, respectively. The same phenomenon occurred in the implanted layer of NC2. However, surface atoms were emitted and randomly reabsorbed on the surface because of the absence of coating during annealing. This behavior was repeated, and we considered that the geometric pattern was hidden by the development of the random granular structure on the surface. The NC2 surface was rougher than the WC2 surface because of the addition of a granular structure to the geometric structure.

For the implanted/annealed SiC damaged by heavy implantation, the implanted layer model of WC2 in Fig. 5 is applicable. In this case, a roughened surface cannot be avoided even if carbon coating is implemented. In contrast, WC1 recovered its 4H-structure and had no rough surfaces. The only difference between WC1 and WC2 was the implantation temperature. Metamorphization of the implanted region and roughened surface structure can be avoided by the prerecovery effect of high-temperature implantation, even after heavy implantation. In this study, rapid thermal annealing was performed at a fixed temperature of 1600 °C. However, the surface structure is expected to be sensitive to the annealing temperature and time. The surface of the high-dose implanted/annealed SiC with carbon coating became rougher as the annealing temperature and time increased.[17,18] The annealing temperature and time are key factors that determine the features of the surface structure of implanted/annealed SiC. It is important to understand the structure of the implanted/annealed SiC and control the implantation and annealing conditions.

V. SUMMARY

In heavily implanted/annealed SiC, the surface is occasionally roughened despite the implementation of carbon coating, which prevents an increase in surface roughness. SPM, DUV Raman spectroscopy, and cross-sectional TEM were used to investigate the effect of carbon-coated annealing on a high-dose implanted/annealed SiC. High-dose implanted SiC samples were prepared at implantation temperatures of 500 and 30 °C, and each implanted sample was subjected to subsequent annealing at 1600 °C with or without carbon coating. Based on the SPM images, the surface of the 500 °C-implanted/annealed SiC sample without coating presented a step-bunching structure reflecting the off-angle, whereas a granular surface was formed in the 30 °C-implanted/annealed SiC sample without coating. These roughened surfaces were attributed to the reabsorption of evaporated surface atoms; in particular, the granular surface resulted from residual implantation damage. In contrast, in the 500 °C-implanted/annealed SiC sample with carbon coating, the flatness of the surface was maintained because of the suppression effect of the coating. However, the surface of the 30 °C-implanted/annealed SiC sample with coating could not prevent an increase in the surface roughness, despite the carbon coating on the surface. Furthermore, the surface exhibited a geometric structure with a lattice pattern in the $\langle 11\bar{2}0\rangle$ directions. This sample had a peak attributed to 3C-SiC and a broad intensity derived from amorphous-SiC in the Raman spectrum. The TEM image of the implanted layer in this sample showed a mixture of 3C-SiC twin domains and amorphous-SiC regions. The 3C-SiC domains presented stacking sequences parallel to the $\langle 110\rangle$ axes, and the $\langle 110\rangle$ axes of 3C-SiC were parallel to the $\langle 11\bar{2}0\rangle$ axes of 4H-SiC. The difference in the thermal expansion coefficients of 3C-SiC and amorphous-SiC resulted in the relative elevation of the 3C-SiC region with respect to that of the amorphous-SiC region after annealing. Furthermore, no granular structures were observed on the surface because surface atoms were not emitted owing to the carbon coating. After the carbon coating was removed, the inner structure of the implanted layer was exposed, thus resulting in a geometric structure on the surface. The roughened surface of the high-dose implanted/annealed SiC with carbon coating was caused by the metamorphized 3C-SiC and amorphous-SiC structures of the implanted layer. Carbon coating during annealing is effective for maintaining the surface flatness of the implanted layer that maintains the 4H-structure; however, it cannot completely suppress the roughened surface in the metamorphosed implanted layer. Competitive prerecovery via high-temperature implantation is essential to prevent the metamorphization of the implanted layer. The high-dose implantation of a SiC crystal requires a careful selection of the appropriate implantation and annealing conditions, even when carbon coating is implemented.

ACKNOWLEDGMENTS

We are thankful to Mr. Y. Yamada and Mr. Y. Wada, former students at Ritsumeikan University, for their help in the TEM experiment. We thank Editage (www.editage.com) for the English language editing. This study did not receive any specific grants from funding agencies in the public, commercial, or nonprofit sectors.

AUTHOR DECLARATIONS

Conflict of Interest

The authors have no conflicts to disclose.

Author Contributions

Kotaro Ishiji: Conceptualization (equal); Data curation (equal); Formal analysis (equal); Investigation (equal); Methodology (equal); Resources (equal); Validation (equal); Writing – original draft (equal). **Makoto Arita:** Methodology (equal); Writing – review & editing (equal). **Mariko Adachi:** Methodology (equal); Writing – review & editing (equal). **Ryuichi Sugie:** Writing – review & editing (equal). **Yukihiro Morita:** Data curation (supporting); Methodology (equal); Writing – review & editing (equal). **Tsutomu Araki:** Methodology (equal); Resources (equal); Writing – review & editing (equal).

DATA AVAILABILITY

Data supporting the findings of this study are included in the article and are available upon reasonable request from the authors.

REFERENCES

[1] M. A. Capano, S. Ryu, M. R. Melloch, J. A. Cooper, Jr., and M. R. Buss, "Dopant activation and surface morphology of ion implanted 4H- and 6H-silicon carbide," J. Electron. Mater. **27**, 370 (1998).

[2] M. A. Capano, S. Ryu, J. A. Cooper, Jr., M. R. Melloch, K. Rottner, S. Karlsson, N. Nordell, A. Powell, and D. E. Walkerm, Jr., "Surface roughening in ion implanted 4H-silicon carbide," J. Electron. Mater. **28**, 214 (1999).

[3] M. V. Rao, J. B. Tucker, M. C. Ridgway, O. W. Holland, N. Papanicolaou, and J. Mittereder, "Ion-implantation in bulk semi-insulating 4H-SiC," J. Appl. Phys. **86**, 752 (1999).

[4] E. M. Handy, M. V. Rao, K. A. Jones, M. A. Derenge, P. H. Chi, R. D. Vispute, T. Venkatesan, N. A. Papanicolaou, and J. Mittereder, "Effectiveness of AlN encapsulant in annealing ion-implanted SiC," J. Appl. Phys. **86**, 746 (1999).

[5] Y. Negoro, K. Katsumoto, T. Kimoto, and H. Matsunami, "Electronic behaviors of high-dose phosphorus-ion implanted 4H-SiC (0001)," J. Appl. Phys. **96**, 224 (2004).

[6] J. Senzaki, S. Harada, R. Kosugi, S. Suzuki, K. Fukuda, and K. Arai, "Improvements in electrical properties of n-type-implanted 4H-SiC substrates using high-temperature rapid thermal annealing," Mater. Sci. Forum **389–393**, 795 (2002).

[7] S. G. Sundaresan, M. V. Rao, Y. Tian, J. A. Schreifels, M. C. Wood, K. A. Jones, and A. V. Davydov, "Comparison of solid-state microwave annealing with conventional furnace annealing of ion-implanted SiC," J. Electron. Mater. **36**, 324 (2007).

[8] A. Wan, S. Huang, M. A. Green, and G. Conibeer, "Rapid thermal annealing and crystallization mechanisms study of silicon nanocrystal in silicon carbide matrix," Nanoscale Res. Lett. **6**, 129 (2011).

[9] W. Weber, "Models and mechanisms of irradiation-induced amorphization in ceramics," Nucl. Instrum. Methods Phys. Res., Sect. B **166**, 98 (2000).

[10] V. Heera, D. Panknin, and W. Skorupa, "p-Type doping of SiC by high dose Al implantation—Problems and progress," Appl. Surf. Sci. **184**, 307 (2001).

[11] J. Wong-Leung, M. K. Linnarsson, B. G. Svensson, and D. J. H. Cockayne, "Ion-implantation-induced extended defect formation in (0001) and $(11\bar{2}0)$ 4H-SiC," Phys. Rev. B **71**, 165210 (2005).

[12] W. J. Weber and F. Gao, "Irradiation-induced defect clustering and amorphization in silicon carbide," J. Mater. Res. **25**, 2349 (2010).

[13] A. Hallén and M. Linnarsson, "Ion implantation technology for silicon carbide," Surf. Coat. Technol. **306**, 190 (2016).

[14] R. Nipoti, H. M. Ayedh, and B. G. Svensson, "Defects related to electrical doping of 4H-SiC by ion implantation," Mater. Sci. Semicond. Proc. **78**, 13 (2018).

[15] K. Ishiji, S. Kawado, Y. Hirai, and S. Nagamachi, "Influence of P^+-implantation and post-annealing on warpage structure of 4H-SiC wafers," Mater. Sci. Forum **778–780**, 449 (2014).

[16] K. Ishiji, S. Kawado, Y. Hirai, and S. Nagamachi, "Resistivity measurement of P^+-implanted 4H-SiC samples prepared at different implantation and annealing temperatures using terahertz time-domain spectroscopic ellipsometry," Mater. Sci. Forum **1004**, 272 (2020).

[17] M. Canino, P. Fedeli, C. Albonetti, and R. Nipoti, "4H-SiC surface morphology after Al ion implantation and annealing with C-cap," J. Microscopy **280**, 229 (2020).

[18] M. Canino, F. Mancarella, F. Bonafe, F. Corticelli, C. Albonetti, and R. Nipoti, "Mechanism governing surface roughening of Al ion implanted 4H-SiC during annealing under a C-cap," Mater. Sci. Forum **1062**, 235 (2022).

[19] S. Potbhare, N. Goldsman, A. Lelis, J. M. McGarrity, F. B. McLean, and D. Habersat, "A physical model of high temperature 4H-SiC MOSFETs," IEEE Trans. Electron Devices **55**, 2029 (2008).

[20] Y. Zhang, W. J. Weber, W. Jiang, C. M. Wang, A. Hallén, and G. Possnert, "Effects of implantation temperature and ion flux on damage accumulation in Al-implanted 4H-SiC," J. Appl. Phys. **93**, 1954 (2003).

[21] Y. Zhang, W. J. Weber, W. Jiang, C. M. Wang, V. Shutthanandan, and A. Hallén, "Effects of implantation temperature on damage accumulation in Al-implanted 4H-SiC," J. Appl. Phys. **95**, 4012 (2004).

[22] K. Ishiji, S. Kawado, Y. Hirai, and S. Nagamachi, "Warpage structure of 4H-SiC after implantation and annealing processes," Mater. Sci. Forum **858**, 544 (2016).

[23] K. Ishiji, K. Sato, T. Fujii, T. Araki, S. Mouri, and R. Sugie, "Correlation between crystal warpage and swelling of 4H-SiC through implantation and annealing," Semicond. Sci. Technol. **35**, 105008 (2020).

[24] H. Harima, "Raman scattering characterization on SiC," Microelectron. Eng. **83**, 126 (2006).

[25] Y. Tamura, M. Nogami, M. Tanaka, T. Maeda, H. Kumasaki, and S. Tamura, "Production implanter Nissin NH-20SR," Nucl. Instrum. Methods Phys. Res., Sect. B **37**, 620 (1989).

[26] Y. Nishimura, A. Chayahara, Y. Horino, and M. Yatsuzuka, "A new PBIID processing system supplying RF and HV pulses through a single feed-through," Surf. Coat. Technol. **156**, 50 (2002).

[27] J. Guy, M. Lodzinski, K. S. Teng, T. G. G. Maffeis, M. Tan, I. Blackwood, P. R. Dunstan, O. Al-Hartomy, S. P. Wilks, T. Wilby, N. Rimmer, D. Lewis, and J. Hopkins, "Investigation of the 4H-SiC surface," Appl. Surf. Sci. **254**, 8098 (2008).

[28] F. Wu, J. Zhang, W. Xi, Y.-Q. Chi, Q.-B. Liu, L. Yang, H.-P. Ma, and Q.-C. Zhang, "Insight into the effects of Al-ion implantation temperature on material properties of 4H-SiC," Appl. Surf. Sci. **613**, 156014 (2023).

[29] S. Nakashima and H. Harima, "Raman investigation of SiC polytypes," Phys. Status Solidi A **162**, 39 (1997).

[30] R. Sugie and T. Uchida, "Determination of stress components in 4H-SiC power devices via Raman spectroscopy," J. Appl. Phys. **122**, 195703 (2017).

[31] E. Oliviero, M. L. David, M. F. Beaufort, J. Nomgaudyte, L. Pranevicius, A. Declémy, and J. F. Barbot, "Formation of bubbles by high dose He implantation in 4H-SiC," J. Appl. Phys. **91**, 1179 (2002).

[32] T. Gorelik, U. Kaiser, C. Schubert, W. Wesch, and U. Glatzel, "Transmission electron microscopy study of Ge implanted into SiC," J. Mater. Res. **17**, 479 (2002).

[33] B. Chen, H. Matsuhata, T. Sekiguchi, K. Ichinoseki, and H. Okumura, "Surface defects and accompanying imperfections in 4H-SiC: Optical, structural and electrical characterization," Acta Mater. **60**, 51 (2012).

[34] M. Diani, L. Simon, L. Kubler, D. Aubel, I. Matko, B. Chenevier, R. Madar, and M. Audier, "Crystal growth of 3C–SiC polytype on 6H-SiC(0 0 0 1) substrate," J. Cryst. Growth **235**, 95 (2002).

[35] S. Nakashima, Y. Nakatake, H. Harima, M. Katsuno, and N. Ohtani, "Detection of stacking faults in 6H-SiC by Raman scattering," Appl. Phys. Lett. **77**, 3612 (2000).

[36] S. Nakashima, T. Mitani, M. Tomobe, T. Kato, and H. Okumura, "Raman characterization of damaged layers of 4H-SiC induced by scratching," AIP Adv. **6**, 15207 (2016).

[37] T. Ohno and N. Kobayashi, "Structure and distribution of secondary defects in high energy ion implanted 4H-SiC," J. Appl. Phys. **89**, 933 (2001).

[38] T. Ohno and N. Kobayashi, "Difference of secondary defect formation by high energy B^+ and Al^+ implantation into 4H-SiC," J. Appl. Phys. **91**, 4136 (2002).

[39] M. F. Beaufort, F. Pailloux, A. Declémy, and J. F. Barbot, "Transmission electron microscopy investigations of damage induced by high energy helium implantation in 4H-SiC," J. Appl. Phys. **94**, 7116 (2003).

[40] S. Sasaki, J. Suda, and T. Kimoto, "Lattice mismatch and crystallographic tilt induced by high-dose ion-implantation into 4H-SiC," J. Appl. Phys. **111**, 103715 (2012).

[41] J. Zhao, L. Ye, X. Jiao, Q. Yue, and Y. Liu, "The damage investigations of 4H-SiC after P-ion irradiation," Appl. Phys. A **126**, 531 (2020).

[42] W. Vetter and M. Dudley, "Characterization of defects in 3C-silicon carbide crystals," J. Cryst. Growth **260**, 201 (2004).

[43] K. Ishiji, M. Kato, and R. Sugie, "Characterization of defect structure in epilayer grown on on-axis SiC by synchrotron X-ray topography," J. Electron. Mater. **51**, 1541 (2022).

[44] S. Leclerc, M. F. Beaufort, A. Declémy, and J. F. Barbot, "Damage induced in high energy helium-implanted 4H-SiC," Nucl. Instrum. Methods Phys. Res., Sect. B **242**, 399 (2006).

[45] S. Rohmfeld, M. Hundhausen, and L. Ley, "Raman scattering in polycrystalline 3C-SiC: Influence of stacking faults," Phys. Rev. B **58**, 9858 (1998).

[46] J. F. Barbot, M. F. Beaufort, M. Texier, and C. Tromas, "Swelling and stacking fault formation in helium implanted SiC," J. Nucl. Mater. **413**, 162 (2011).

[47] M. Marinova, A. Andreadou, A. Mantzari, and E. K. Polychroniadis, "On the twin boundary propagation in (111) 3C-SiC layers," Mater. Sci. Forum **717–720**, 419 (2012).

[48] T. Yamashita, H. Matsuhata, T. Sekiguchi, K. Momose, H. Osawa, and M. Kitabatake, "Characterization of comet-shaped defects on C-face 4H-SiC epitaxial wafers by electron microscopy," J. Cryst. Growth **416**, 142 (2015).

[49] D. N. Talwar and J. C. Sherbondy, "Thermal expansion coefficient of 3C-SiC," Appl. Phys. Lett. **67**, 3301 (1995).

[50] T. Chikada, A. Suzuki, and T. Terai, "Deuterium permeation and thermal behaviors of amorphous silicon carbide coatings on steels," Fusion Eng. Des. **86**, 2192 (2011).

[51] H. Zang, D. Guo, T. Shen, C. He, Z. Wang, L. Pang, C. Yao, and T. Yang, "Investigation of swelling induced by heavy ion and neutron irradiation in SiC," J. Nucl. Mater. **433**, 378 (2013).